International Journal of Nanomedicine

Dovepress
open access to scientific and medical research

Open Access Full Text Article

ORIGINAL RESEARCH

Hyperthermia mediated by dextran-coated $La_{0.7}Sr_{0.3}MnO_3$ nanoparticles: in vivo studies

This article was published in the following Dove Press journal:
International Journal of Nanomedicine
27 April 2016
Number of times this article has been viewed

Reihaneh Haghniaz
Rinku D Umrani
Kishore M Paknikar

Centre for Nanobioscience, Agharkar Research Institute, Pune, India

Purpose: The aim of this study was to evaluate radiofrequency-induced dextran-coated lanthanum strontium manganese oxide nanoparticles-mediated hyperthermia to be used for tumor regression in mice.

Materials and methods: Nanoparticles were injected intra-tumorally in melanoma-bearing C57BL/6J mice and were subjected to radiofrequency treatment.

Results: Hyperthermia treatment significantly inhibited tumor growth (~84%), increased survival (~50%), and reduced tumor proliferation in mice. Histopathological examination demonstrated immense cell death in treated tumors. DNA fragmentation, increased terminal deoxynucleotidyl transferase-dUTP nick end labeling signal, and elevated levels of caspase-3 and caspase-6 suggested apoptotic cell death. Enhanced catalase activity suggested reactive oxygen species-mediated cell death. Enhanced expression of heat shock proteins 70 and 90 in treated tumors suggested the possible development of "antitumor immunity".

Conclusion: The dextran-coated lanthanum strontium manganese oxide-mediated hyperthermia can be used for the treatment of cancer.

Keywords: lanthanum strontium manganese oxide nanoparticles, melanoma, tumor regression, survival, heat shock proteins, MRI

Introduction

Many aggressive cancers, such as melanoma, are relatively resistant to chemotherapeutic drugs.[1] Failure to treat these types of cancers by conventional therapy has enthused interest in the development of newer strategies.[2] Hyperthermia or heat therapy (typically to the tune of 41°C–47°C) is a promising strategy to combat cancers.[3] Tumor tissues are reported to be more susceptible to high temperatures as compared to normal tissues due to impaired heat dissipation.[4,5] Thus, hyperthermia can destroy the tumor tissues while sparing the healthy ones.[5,6] However, it is often not possible to heat the tumor cells selectively as conventional hyperthermia involves applying heat to the entire body.[7] To overcome this difficulty, magnetic nanoparticles (MNP)-mediated hyperthermia, which results in localized heating, is being developed as a method of choice.[8–11]

To achieve localized heating, biocompatible MNPs are deposited in the tumor and exposed to an alternating magnetic field, that is, radiofrequency (RF). The absorbed energy results in rapid flipping of magnetic moments and subsequent heat generation.[11] Since heat is generated only at the location of MNPs, this therapy can minimize heat-induced damage to other healthy tissues surrounding the tumor. Moreover, as MNPs cannot be heated beyond their Curie temperature, controlled heating can be achieved. Selecting MNPs with low Curie temperature allows self-controlled heating in the therapeutic range (41°C–47°C) and minimizes adverse effects of the therapy.[12]

Correspondence: Rinku D Umrani; Kishore M Paknikar
Centre for Nanobioscience, Agharkar Research Institute, GG Agarkar Road, Pune 411004, Maharashtra, India
Tel +91 20 2532 5127;
+91 20 2532 5001
Fax +91 20 2565 1542
Email rinkuumrani@aripune.org; kpaknikar@gmail.com

submit your manuscript | www.dovepress.com
Dovepress
http://dx.doi.org/10.2147/IJN.S104617

One such example of MNPs with low Curie temperature is ferromagnetic lanthanum strontium manganese oxide (LSMO) nanoparticles. We have earlier reported that dextran-coated $La_{0.7}Sr_{0.3}MnO_3$ (Dex-LSMO) nanoparticles (30–50 nm) with Curie temperature of ~360 K (~86°C) show self-controlled heating property and have potential to be used for both localized hyperthermia[13,14] and magnetic resonance imaging (MRI).[15] Although iron oxide nanoparticles (magnetite/maghemite) are extensively studied for hyperthermia, the heating is not self-controlled in the therapeutic range owing to their high Curie temperature. Thus, LSMO nanoparticles offer a distinct advantage over the commonly used magnetite nanoparticles. In our previous study, a temperature of ~45°C was found to be optimum for apoptotic cell death and induction of heat shock proteins (HSPs) in a murine melanoma cell line (B16F1).[16] In vitro cancer cell-killing effect[16,17] and the lack of toxicity after administration of Dex-LSMO nanoparticles in mice, observed in the earlier study,[15] confirmed the possible application of these nanoparticles for in vivo hyperthermia.

Despite several in vitro reports demonstrating the potential ability of LSMO nanoparticles in cancer treatment,[18–20] studies on in vivo tumor regression have not yet been attempted. The present study seeks to fill this knowledge gap by evaluating RF-induced Dex-LSMO nanoparticles-mediated hyperthermia to be used for tumor regression in melanoma-bearing C57BL/6J mice.

Materials and methods

Synthesis and characterization of Dex-LSMO nanoparticles

$La_{0.7}Sr_{0.3}MnO_3$ nanoparticles were prepared by citrate gel method using stoichiometric amounts of metal acetate hydrate precursors.[13,14] LSMO nanoparticles were then coated with dextran sulfate sodium salt to improve biocompatibility as reported earlier.[14] These Dex-LSMO nanoparticles were then characterized using dynamic light scattering (Model Delsa™Nano; Beckman Coulter Incorporation, Brea, CA, USA), high-resolution transmission electron microscopy (Model TECNAI-T30; FEI Company, Hillsboro, OR, USA), thermogravimetric analysis (Model TGA-7; PerkinElmer Inc., Waltham, MA, USA), and vibrating sample magnetometry (Model EG and G 4500; Princeton Applied Research Corporation, Princeton, NJ, USA).

Cell culture

A murine melanoma (B16F1) cell line was procured from National Center for Cell Sciences (Pune, India). Dulbecco's Modified Eagle's Medium (DMEM) and fetal bovine serum were purchased from Invitrogen (Carlsbad, CA, USA). Antibiotic antimycotic solution 100× and trypsin phosphate versene glucose were procured from HiMedia Laboratories (Mumbai, India). Cells were grown in tissue culture flasks (25 cm^2) containing DMEM supplemented with 10% fetal bovine serum and 1% antibiotic antimycotic solution, and were maintained at 37°C and 5% CO_2 atmosphere.

Animal husbandry

All animal experiments were conducted after approval by the Institutional Animal Ethics Committee of Agharkar Research Institute, Pune, India. Animal handling procedures were carried out as per institutional guidelines with humane care as mentioned in the Committee for the Purpose of Control and Supervision of Experiments on Animals guidelines, Ministry of Environment and Forests, Government of India.

C57BL/6J mice (8–10 weeks old) were procured from Advanced Centre for Treatment, Research and Education in Cancer (Mumbai, India). After arrival, the mice were allowed to acclimatize for 1 week. During the acclimatization and experimental periods, the mice were housed under 12 hour:12 hour light:dark cycle, at 22°C±3°C temperature and 60%±10% relative humidity in pathogen-free conditions. Standard laboratory pellet feed and purified water were provided ad libitum.

Tumor induction in mice

To induce superficial melanoma, B16F1 cell suspension (1×10^5 cells in 100 µL serum-free DMEM) was subcutaneously injected in the shaved flank region of C57BL/6J mice. When the tumor nodule was palpable (~21 days), its growth was monitored every alternate day using a digital Vernier caliper. Tumor volume was calculated using the following formula:

$$\text{Tumor volume} = (\text{length} \times \text{width}^2) \times 0.5$$

Mice bearing sufficiently large tumors (~1.6×10^3 mm^3 volume) were used for further experiments.

Tissue distribution of Dex-LSMO nanoparticles

Qualitative assessment of tissue distribution of Dex-LSMO nanoparticles was carried out using MRI. Melanoma-bearing mice were divided randomly into four groups (n=6 for each group). Three groups of mice were injected with Dex-LSMO nanoparticles (5 mg in 100 µL saline) at the site of tumor,

and euthanized at 24, 48, or 72 hours after injection. The fourth group of mice were injected with saline and served as a control. Various tissues, viz tumor, liver, lung, kidneys, heart, and spleen, were visualized using clinical MRI scanner (Model 1.0 T Signa scanner; General Electric Medical Systems, Milwaukee, WI, USA). Spin echo T_2-weighted images were captured (parameters used: echo time =99 ms, repetition time =3,000 ms, slice thickness =7 mm, field of view =24×24 cm, matrix =320×192, flip angle =90°, and imaging time =1.0 minute).

Quantitative assessment of tissue distribution of Dex-LSMO nanoparticles was performed by atomic absorption spectrometry. Melanoma-bearing mice were divided into four groups (n=6 for each group). Dex-LSMO nanoparticles (5 mg in 100 µL saline) were injected at the site of tumor, and mice were euthanized at 0, 24, 48, or 72 hours after injection. Tissues (tumor, liver, lung, kidneys, heart, and spleen) were dissected, weighed, and acid-digested (in a 1:1 mixture of concentrated hydrochloric acid and sulfuric acid). Levels of strontium (Sr [Strontium], a representative element for LSMO) in the digested tissue samples were estimated using an atomic absorption spectrometer (Model Analyst 800; PerkinElmer, Waltham, MA, USA). These data were further used to calculate percent retention and distribution of Dex-LSMO nanoparticles in tumors and healthy tissues, respectively. Results obtained were evaluated by two-way analysis of variance where $P<0.05$ was considered as minimal level of significance.

Hyperthermia treatment experimental design

Melanoma-bearing mice (tumor volume ~1.6×10^3 mm^3) were divided into four different groups, 20 mice in each group. The groups were designated as: (i) saline control, (ii) Dex-LSMO control, (iii) saline + RF control, and (iv) Dex-LSMO + RF-treated. Before treatment, all mice were anesthetized using ketamine and xylazine cocktail (50 mg/kg dose of each drug). Intra-tumoral injections of saline (100 µL) and Dex-LSMO nanoparticles (5 mg in 100 µL saline) were given to mice in groups (i) and (iii), and groups (ii) and (iv), respectively. Subsequently, mice in groups (iii) and (iv) were shifted to a restrainer placed in a water-cooled induction coil (50 mm internal diameter, five turns) and were exposed to RF (365 kHz, 700 A, 8,000 W) for 20 minutes on Day 0, Day 3, and Day 6. Mice in groups (i) and (ii) were not exposed to RF. During the treatment, intra-tumoral and body (rectal) temperatures were monitored simultaneously using custom-made 1 mm temperature probes (PT100; Hi-Tech Transducers and Devices, Pune, India). The 20 mice of each treatment group were subsequently divided into three subsets for evaluation of different parameters. Tumor growth and survival time were monitored in the first subset of mice (n=10 per group). The second subset of mice (n=6 per group) were sacrificed on Day 8, and tissues were collected and processed for histopathological examination. The third subset of mice (n=4 per group) were also sacrificed on Day 8, and tissues were collected and processed to analyze cell proliferation, cell death, inflammatory responses, antioxidant status, and HSPs induction. The treatment regimen used is illustrated in Figure 1.

Tumor growth monitoring and survival time

Tumor volumes in experimental mice (from subset I) were measured every alternate day from Day 0 to Day 14. Percent tumor growth inhibition (T_{in}) on Day 14 was calculated using the following formula:

$$T_{in} = 1 - \frac{\text{Average tumor volume in group (iv)}}{\text{Average tumor volume in group (i)}} \times 100$$

Data are presented as mean ± standard error of the mean. Statistical analysis was performed by one-way analysis of variance followed by Dunnett's multiple comparison test where $P<0.05$ was considered as minimal level of significance.

All experimental mice (of subset I) were not sacrificed and observed until mortality. Based on these observations, Kaplan–Meier survival curves were generated using GraphPad Prism software (version 5; GraphPad Software Incorporation, La Jolla, CA, USA). Statistical significance was analyzed by log rank test where a value of $P<0.05$ was considered as the minimal level of significance. Percent increase in life expectancy was calculated as follows:

$$\text{\% increase in life expectancy} = \frac{\text{Survival}_{\text{treated}} - \text{Survival}_{\text{control}}}{\text{Survival}_{\text{control}}} \times 100$$

Histopathological examination

Excised tumors and livers (as a representative healthy tissue surrounding tumor) from mice of subset II were fixed in 10% formalin, embedded in paraffin, sectioned (5–7 µm thick), deparaffinized, and stained with hematoxylin–eosin. Sections were imaged using an optical microscope (Model Eclipse E200; Nikon, Tokyo, Japan).

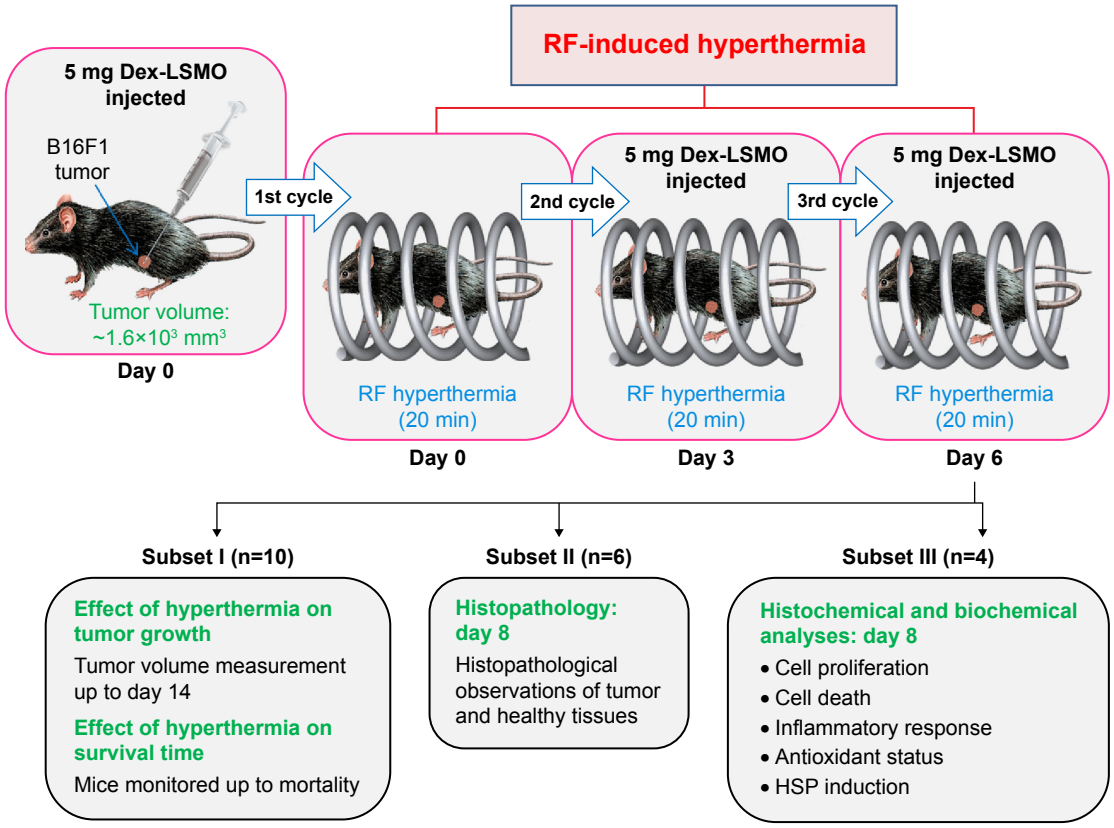

Figure 1 RF-induced hyperthermia: experimental design.
Abbreviations: Dex-LSMO, dextran-coated lanthanum strontium manganese oxide; RF, radiofrequency; HSP, heat shock protein.

Assessment of tumor proliferation

Tumor sections excised from mice of subset III were deparaffinized, blocked, and incubated with monoclonal Ki-67 primary antibody (1:300 dilution; Thermo Fisher Scientific, Waltham, MA, USA) for 1 hour. The sections were then incubated with HRP-IgG (1:300 dilution; Bangalore Genei, Bangalore, India) for 1 hour, followed by incubation with 3,3′-diaminobenzidine hydrochloride (Bangalore Genei) substrate for 30 minutes in the dark. Cells were counterstained using hematoxylin (1:50 dilution in distilled water) for 1 hour. Slides were then imaged with an optical microscope.

Apoptosis assessment by TUNEL assay

Apoptosis in tumor and liver sections (of subset III mice) was assessed by terminal deoxynucleotidyl transferase-dUTP nick end labeling (TUNEL) staining using In Situ Cell Death Detection Kit-Fluorescein (Roche Diagnostics, Basel, Switzerland). Tissue sections were deparaffinized, blocked, and incubated with TUNEL reaction mixture for 60 minutes in the dark. Tissue sections were then counterstained with Hoechst 33342 (50 µg/mL; Invitrogen) for 20 minutes to stain nuclei. Subsequently, slides were washed with phosphate-buffered saline, mounted, and visualized under a fluorescence microscope (Eclipse E200; Nikon). Images were merged using Image-Pro plus software (Version 6; Media Cybernetics Inc., Rockville, MD, USA) to confirm colocalization of TUNEL signal (green) with nuclei (blue).

Apoptosis assessment by DNA laddering assay

DNA was isolated from tumors (of subset III mice) using GenElute Mammalian Genomic DNA Miniprep Kit (Bangalore Genei) according to the manufacturer's instructions. Isolated DNA samples (20 µL aliquots) were then loaded on 1% agarose gel and electrophoresed at 90 V for 1.5 hours. DNA bands on the gel were visualized under Ultra Violet (UV) light and compared with a DNA ladder (Lambda DNA/EcoRI + HindIII; Thermo Fisher Scientific).

Apoptosis assessment by caspase assay

Tumor and liver samples (of subset III mice) were homogenized in radioimmunoprecipitation assay buffer containing protease inhibitor cocktail (Sigma Aldrich Corporation, St Louis, MO, USA) according to the manufacturer's instructions. Protein concentrations were determined by Bradford assay. Activity of caspase-2, caspase-3, caspase-6, caspase-8,

and caspase-9 was measured in tissue lysates using Caspase Colorimetric Protease Assay Sampler Kit (Invitrogen). Absorbance at 405 nm was recorded using a microplate reader (Model Synergy HT Multi-Mode; BioTek Instruments Incorporation, Winooski, VT, USA), and fold change as compared to control was calculated. Statistical analysis was performed using unpaired Student's *t*-test where $P<0.05$ was considered as the minimal level of significance.

Evaluation of pro-inflammatory cytokines

Interleukin-1α (IL-1α) and tumor necrosis factor-α (TNF-α) levels in the tumor and liver lysates (of subset III mice) were quantified using Enzyme Linked Immunosorbent Assay (ELIZA) kits (Signosis, Sunnyvale, CA, USA) as per manufacturer's instructions. Absorbance at 450 nm was determined using a microplate reader. IL-1α and TNF-α levels of samples were obtained from the standard curve. Statistical analysis was performed using unpaired Student's *t*-test where $P<0.05$ was considered as the minimal level of significance.

Evaluation of antioxidant activity

Catalase and superoxide dismutase (SOD) activity of tumor and liver lysates (of subset III mice) was estimated using standard kits (Cayman Chemicals, Ann Arbor, MI, USA) following manufacturer's instructions. Statistical significance was tested using unpaired Student's *t*-test where $P<0.05$ was considered as the minimal level of significance.

Evaluation of HSP70 and HSP90 induction

Quantitative evaluation of constitutive and inducible HSP70 and HSP90 in tumor and liver lysates (of subset III mice) was performed by indirect ELISA method. In brief, tissue lysates or HSP standards (ranging from 2 to 15 µg/mL; Sigma Aldrich Corporation) were dispensed into 96-well microtiter plates and incubated overnight at 4°C. After washing and blocking steps, optimized concentration of Monoclonal Anti-Heat Shock Protein 70 antibody (1:5,000 dilution) or Monoclonal Anti-Heat Shock Protein 90 antibody (1:2,000 dilution) antibody (Sigma Aldrich Corporation) was added to respective wells, and the plate was incubated for 2 hours. Subsequently, wells were washed, and HRP-IgG antibody (1:5,000 dilution) was added. After 2 hours, wells were washed, and 3,3′,5,5′-Tetramethylbenzidine-H_2O_2 substrate (Sigma Aldrich Corporation) was added. The plate was incubated in the dark (~15 minutes) until the development of blue color. Thereafter, H_2SO_4 (12%) was added to stop the reaction. Absorbance at 450 nm was measured using a microplate reader. Concentration of HSPs in the samples was determined using standard plots and presented as microgram HSPs/milligram protein. Statistical significance was tested using unpaired Student's *t*-test where $P<0.05$ was considered as the minimal level of significance.

Results

Synthesis and characterization of Dex-LSMO nanoparticles

The synthesized Dex-LSMO nanoparticles had a narrow particle size distribution (25–50 nm) with a zeta potential of −40 mV. Thermogravimetric analysis revealed the presence of ~23% dextran in Dex-LSMO nanoparticles. Vibrating sample magnetometry analysis showed ferromagnetic nature of synthesized nanoparticles with a Curie temperature of ~360 K.

Tissue distribution of Dex-LSMO nanoparticles

Processed MR images (Figure 2, panel B) of collected tissues show the distribution of Dex-LSMO nanoparticles. To get a clear idea about the tissue dimensions, actual photographs of the excised tissues are also shown (Figure 2, panel A). As can be seen from the MR images of control animals (not injected with Dex-LSMO nanoparticles), all the tissues appeared bright. As expected, 24 hours after intra-tumoral injection, the tumor looked completely dark, due to the presence of nanoparticles. Reduction of signal intensity (ie, darkness) was observed in the lung and spleen at 24 hours, suggesting accumulation of nanoparticles in these tissues. Other tissues such as the liver, kidney, and heart showed no change in signal intensity indicating no or negligible accumulation of nanoparticles. The tumor, lung, and spleen tissues showed gradual clearance of nanoparticles at 48 and 72 hours post-injection, as seen by increasing signal intensity.

It can be clearly seen from Figure 3A that strontium concentrations in tumor declined with time, reaching up to 40% of the injected dose by 72 hours. Sr concentrations in the healthy tissues, viz the liver, lung, kidney, heart, and spleen, were negligible (≤2%) at all the time points (Figure 3B) as compared to tumor Sr concentrations measured at 0 hour. These results were in agreement with qualitative data obtained using MRI vide supra.

Effect of RF-induced Dex-LSMO nanoparticles-mediated hyperthermia treatment on tumor growth and survival time

It was seen that RF-induced Dex-LSMO nanoparticles-mediated hyperthermia raised the intra-tumoral temperature to ~45°C within 6 minutes. The tumor temperature remained

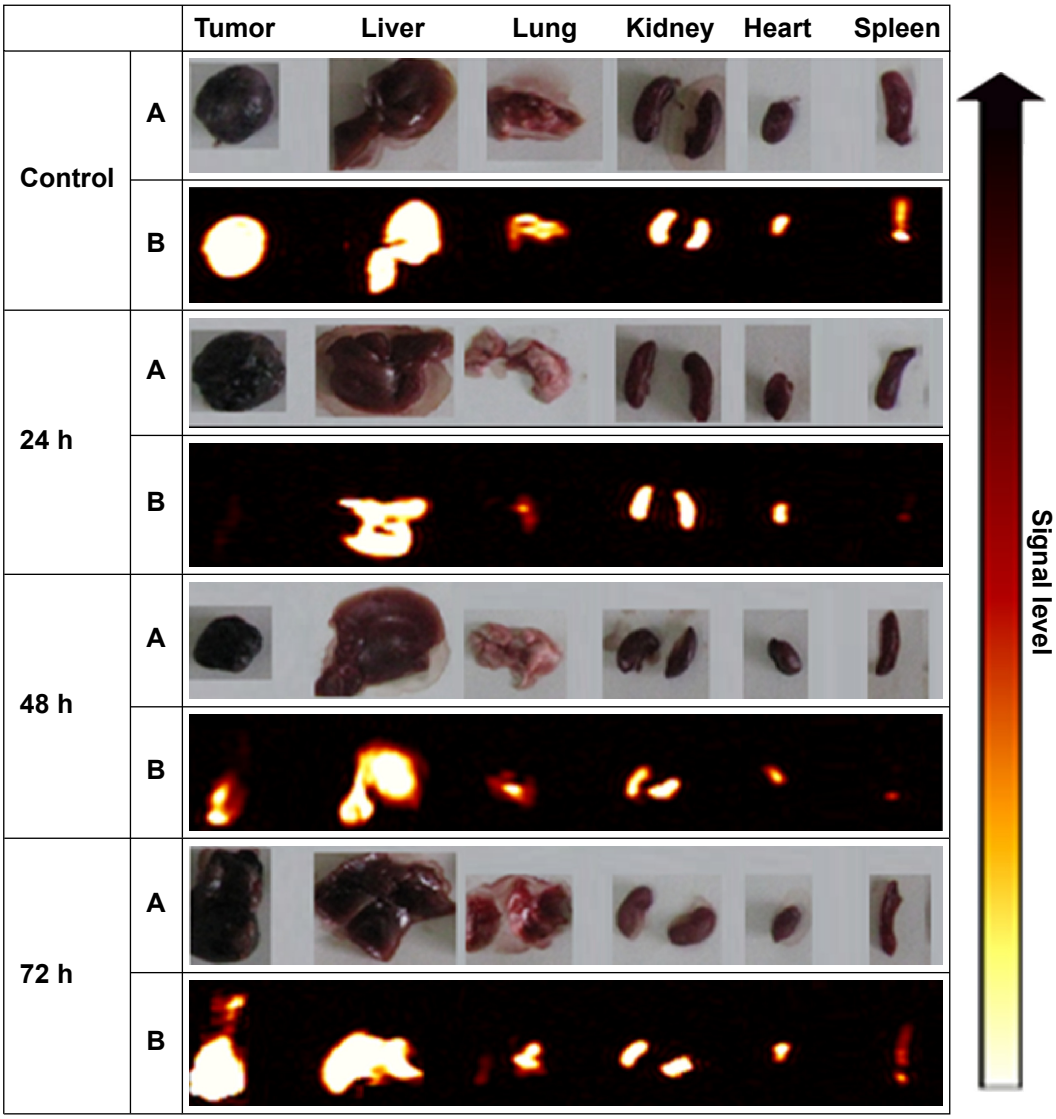

Figure 2 Qualitative assessment of Dex-LSMO nanoparticles distribution by magnetic resonance imaging.
Notes: Photographs (panel A) and processed ex vivo MR images (panel B) of representative tissues at different time points after intra-tumoral injection of Dex-LSMO nanoparticles. The gradient color bar on right indicates the signal level emanated by nanoparticles (lighter: lower concentration of nanoparticles; darker: higher concentration of nanoparticles).
Abbreviations: MR, magnetic resonance; Dex-LSMO, dextran-coated lanthanum strontium manganese oxide.

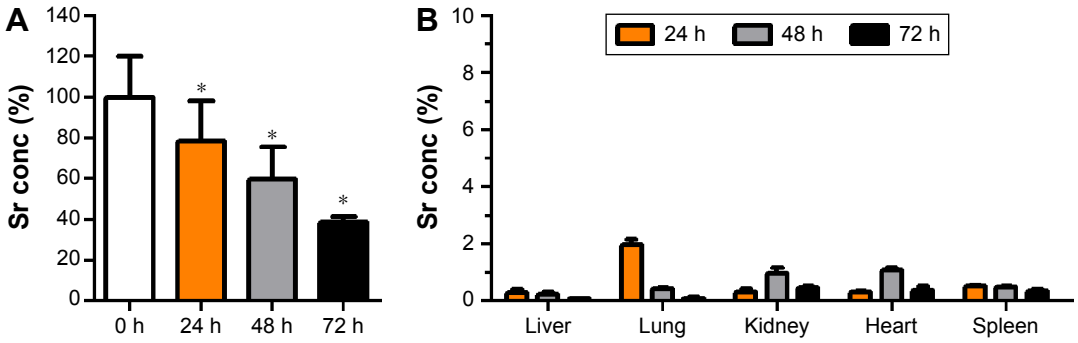

Figure 3 Quantitative assessment of Dex-LSMO nanoparticles distribution by atomic absorption spectroscopy.
Notes: Percent concentration of strontium (Sr conc) estimated at different time points (**A**) in tumor and (**B**) in different healthy tissues. *$P<0.05$ as analyzed by two-way ANOVA. Data are presented as mean ± SEM.
Abbreviations: ANOVA, analysis of variance; SEM, Standard error of the mean; Dex-LS MO, dextran-coated lanthanum strontium manganese oxide.

unaltered until the end of the treatment (ie, for 20 minutes). After switching off the RF, the temperature returned to normal body temperature (~35°C) within 5 minutes. In saline + RF control group, tumor temperature remained elevated by ~1°C above the normal body temperature during exposure to RF. Moreover, the rectal temperature in both control and treatment groups remained ~36°C during RF exposure.

Representative photographs of melanoma-bearing mice (taken on Day 10) are presented in Figure 4A. It was observed that tumor volume in the control groups increased from ~1.6×10^3 to ~17×10^3 mm^3 by Day 14, whereas tumor volume of Dex-LSMO + RF-treated mice was ~2.6×10^3 mm^3 (Figure 4B). Tumor growth inhibition percentage was found to be 84.2% in Dex-LSMO + RF-treated group (Figure 4C). No significant growth inhibition was observed in Dex-LSMO control and saline + RF control groups, suggesting that neither nanoparticles nor RF has any stand-alone treatment value.

As can be seen from Figure 4D, survival at the start of the treatment was 100% in all the groups. All mice in the control groups (saline, Dex-LSMO, and saline + RF groups) died by Day 18. Mice in Dex-LSMO + RF-treated group survived noticeably longer, that is, up to Day 23. The average survival of the mice in the Dex-LSMO + RF-treated group obtained from Kaplan–Meier survival curve was found to be 21 days in comparison to 14 days in saline control group. Thus, a prolonged survival of 7 days was seen after hyperthermia treatment (ie, 50% increase in life expectancy).

Effect of RF-induced Dex-LSMO nanoparticles-mediated hyperthermia treatment on tumor histology

Representative photomicrographs of tumors from control groups and Dex-LSMO + RF-treated group are shown in Figure 5A. Immense cell death (necrotic areas shown as asterisks) was evidenced in Dex-LSMO + RF-treated tumors. There was no evidence of any damage in the tumors of Dex-LSMO control and saline + RF control groups, indicating that RF or Dex-LSMO nanoparticles alone do not have any therapeutic value. Moreover, no differences were seen in the characteristic histological appearance of the liver tissues in all the

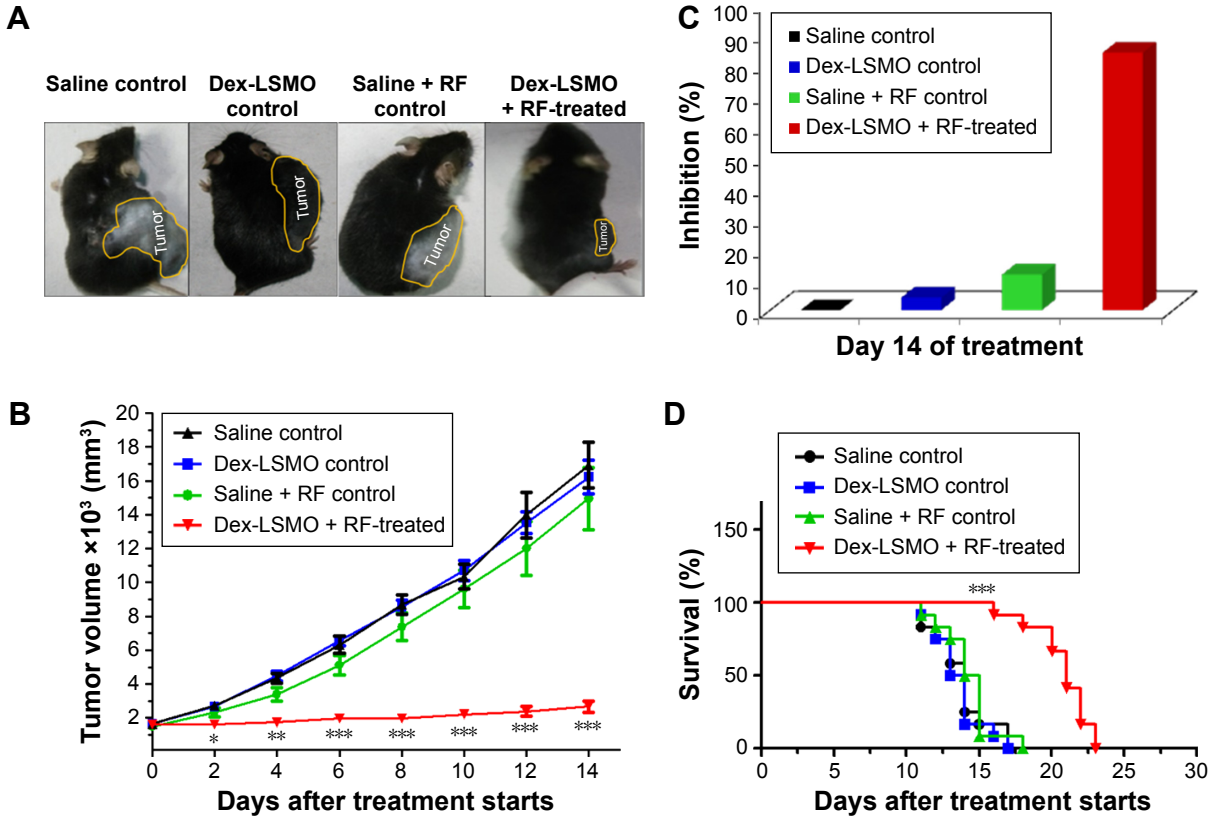

Figure 4 Effect of RF induced Dex-LSMO nanoparticles-mediated hyperthermia treatment on tumor growth and survival time.
Notes: (**A**) Photograph of melanoma-bearing mice in control and Dex-LSMO + RF-treated groups on Day 10. (**B**) Tumor volume of mice after treatment with Dex-LSMO-mediated hyperthermia as compared to control groups. *$P<0.05$, **$P<0.01$, and ***$P<0.001$ as analyzed by one-way ANOVA followed by Dunnett's multiple comparison test. (**C**) Tumor inhibition percentage in different groups of mice on Day 14. (**D**) Kaplan–Meier survival curves of control and Dex-LSMO + RF-treated groups of mice. ***$P<0.001$ as analyzed by log rank test. Data are presented as mean ± SEM.
Abbreviations: Dex-LSMO, dextran-coated lanthanum strontium manganese oxide; RF, radiofrequency; ANOVA, analysis of variance; SEM, Standard error of the mean.

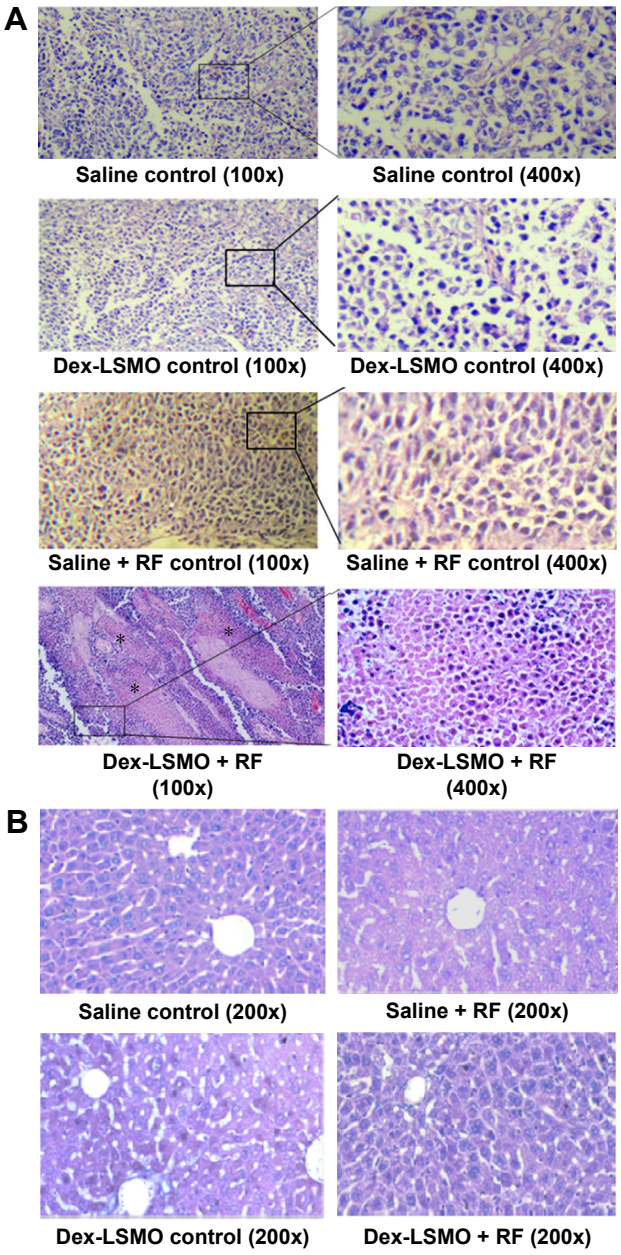

Figure 5 Effect of RF induced Dex-LSMO nanoparticles-mediated hyperthermia treatment on tumor histology.
Notes: Photomicrographs of HE-stained (**A**) tumor sections and (**B**) liver sections from untreated controls and Dex-LSMO + RF-treated mice on Day 8 of treatment. Asterisks show necrotic area.
Abbreviations: HE, hematoxylin and eosin; Dex-LSMO, dextran-coated lanthanum strontium manganese oxide; RF, radiofrequency.

controls and Dex-LSMO + RF-treated mice (Figure 5B), suggesting no risk of cell death in surrounding healthy tissues.

Effect of RF-induced Dex-LSMO nanoparticles-mediated hyperthermia treatment on tumor proliferation

Figure 6 shows the images of Ki-67 staining in tumor sections of Dex-LSMO + RF-treated mice as compared to saline control. Light-to-dark brown spots that colocalized in nuclei (stained blue) were considered as positive for Ki-67 expression. It could be seen that the expression of Ki-67 was significantly reduced in the treated group as compared to control.

Apoptosis assessment by TUNEL assay

Figure 7A depicts the representative fluorescent images of tumor and liver sections collected from saline control and Dex-LSMO + RF-treated mice. Very few apoptotic cells (green signal) could be seen in the tumor of the saline control group, whereas hyperthermia treatment resulted in significant apoptosis. No difference in TUNEL signal was noted in the liver sections of treated animals as compared to controls.

Apoptosis assessment by DNA laddering assay

DNA fragmentation was detected in Dex-LSMO + RF-treated group (Figure 7B), indicating apoptotic cell death. In contrast, none of the control groups showed any DNA fragmentation.

Apoptosis assessment by caspase assay

Executive caspase-3 and caspase-6 levels increased by ~2- and ~1.6-fold, respectively, in tumors of treated mice (Figure 7C). The level of initiator caspases (ie, caspase-2, caspase-8, and caspase-9) also increased; however, the difference was not statistically significant. In contrast to the tumor tissue, the activity of all tested caspases was unaltered in the liver of treated animals.

Effect of RF-induced Dex-LSMO nanoparticles-mediated hyperthermia treatment on inflammatory responses

To investigate the possible role of pro-inflammatory cytokines in apoptotic cell death following hyperthermia, expression of IL-1α and TNF-α was evaluated. As can be seen in Figure 8A and B, levels of IL-1α and TNF-α in tumor of Dex-LSMO + RF-treated mice were not significantly different from control mice, suggesting that these cytokines may not play a role in induction of cell death by Dex-LSMO nanoparticles-mediated hyperthermia. These levels were also unaltered in the liver tissue of treated mice as compared to controls.

Evaluation of antioxidant activity

As shown in Figure 8C, SOD activity in treated tumors was not altered as compared to control. Likewise, no appreciable changes in SOD activity were found in the liver of treated animals. As can be seen in Figure 8D, catalase activity significantly increased in treated tumors as compared to

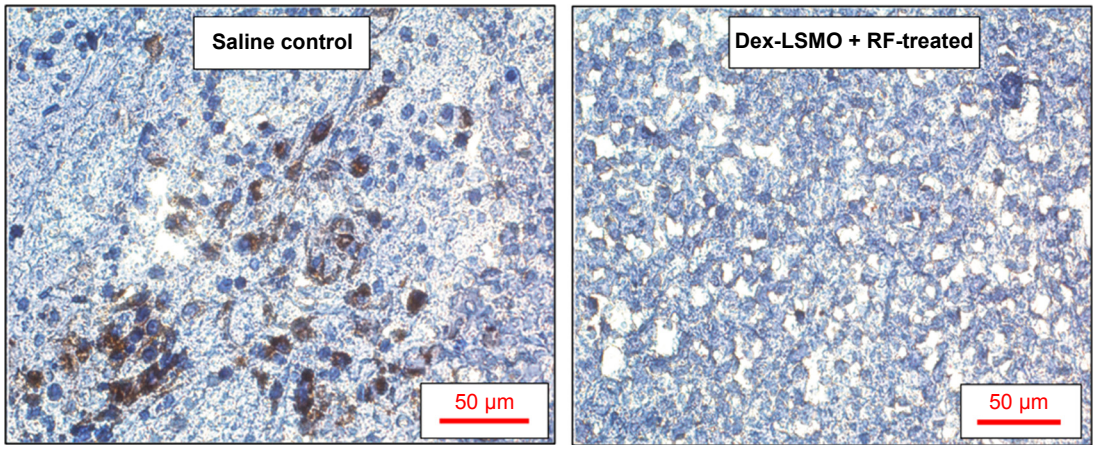

Figure 6 Effect of RF induced Dex-LSMO nanoparticles-mediated hyperthermia treatment on tumor proliferation.
Notes: Representative photomicrographs of Ki-67-stained tumor sections of saline control and Dex-LS MO + RF-treated mice.
Abbreviations: Dex-LSMO, dextran-coated lanthanum strontium manganese oxide; RF, radiofrequency.

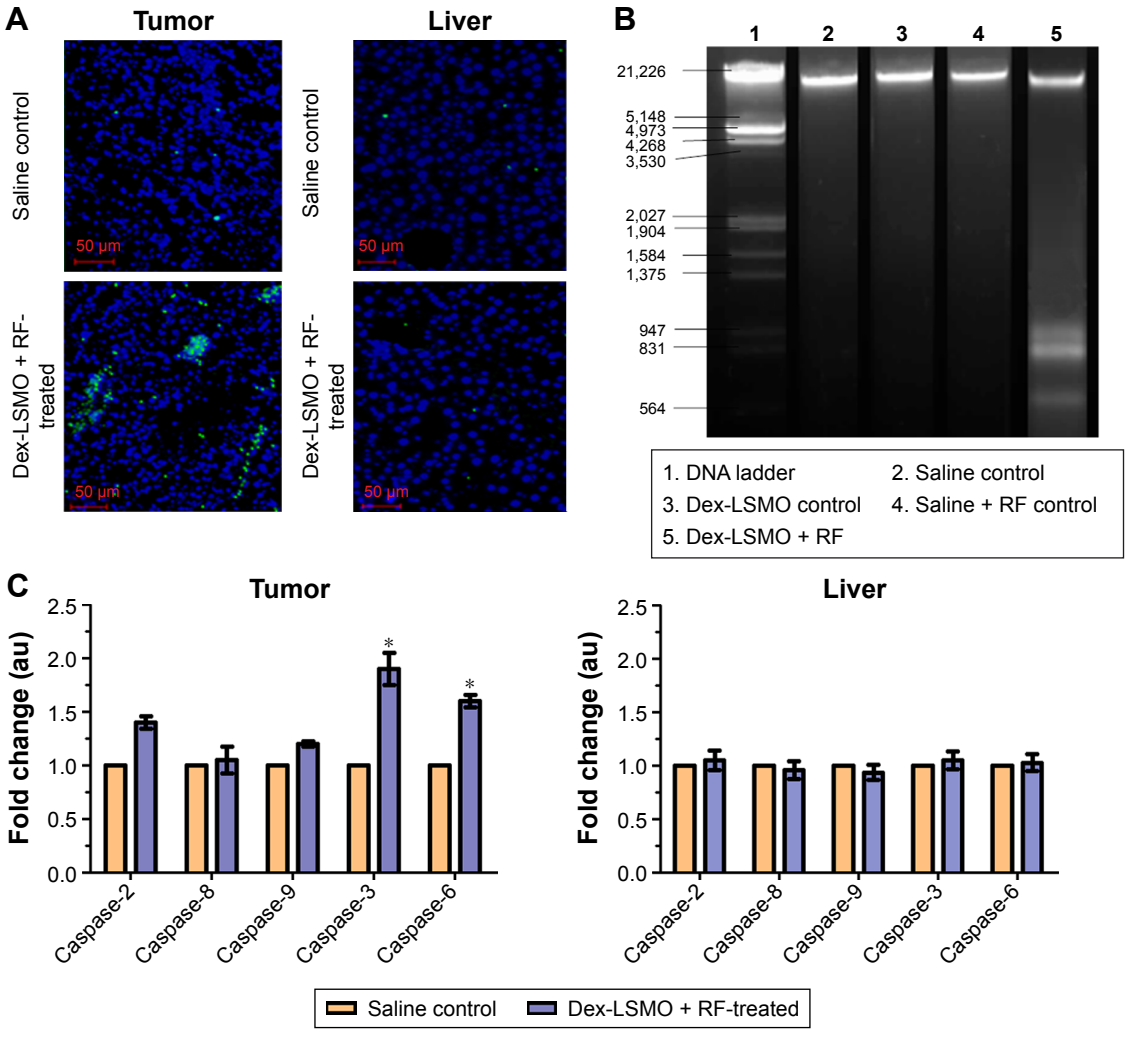

Figure 7 Assessment of apoptotic cell death after hyperthermia treatment.
Notes: (**A**) Representative images of TUNEL-positive apoptotic cells in tumor and liver sections of saline control and Dex-LSMO + RF-treated mice. (**B**) Agarose gel electrophoresis of DNA isolated from tumor of control and Dex-LSMO + RF-treated mice. (**C**) Caspase activity in tumor and liver tissues of saline control and Dex-LSMO + RF-treated mice. *$P<0.05$ as analyzed by unpaired Student's *t*-test.
Abbreviations: TUNEL, terminal deoxynucleotidyl transferase-dUTP nick end labeling; Dex-LSMO, dextran-coated lanthanum strontium manganese oxide; RF, radiofrequency.

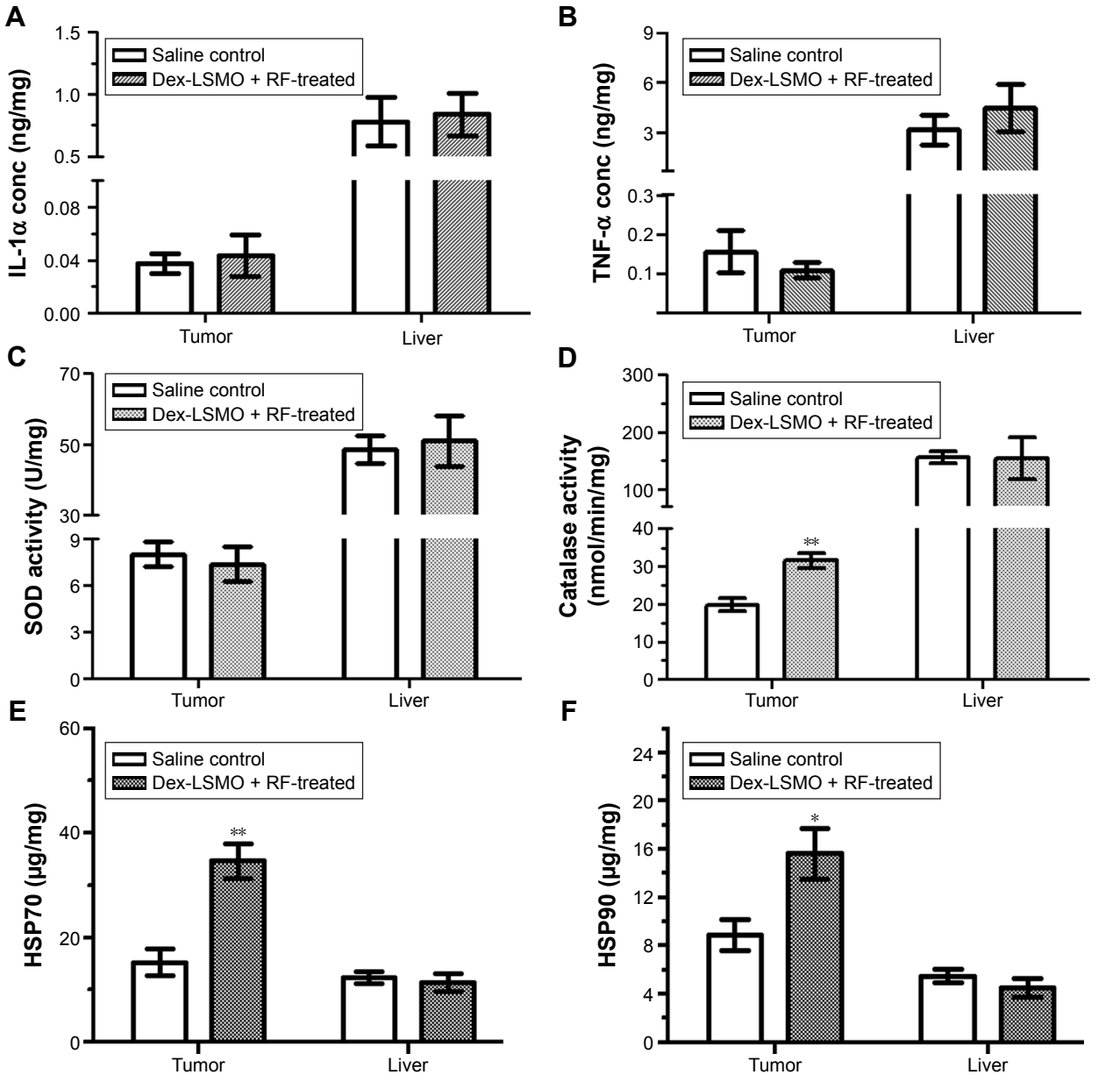

Figure 8 Effect of RF induced Dex-LSMO nanoparticles-mediated hyperthermia treatment on biochemical parameters.

Notes: Levels of (**A**) IL-1α and (**B**) TNF-α in tumor and liver of saline control and Dex-LSMO + RF-treated mice. (**C**) SOD and (**D**) catalase activity in tumor and liver of saline control and Dex-LSMO + RF-treated mice. Levels of (**E**) HSP70 and (**F**) HSP90 in tumor and liver of saline control and Dex-LSMO + RF-treated mice. *$P<0.05$ and **$P<0.01$ as analyzed by unpaired Student's *t*-test.

Abbreviations: IL-1α, interleukin-1α; TNF-α, tumor necrosis factor-α; Dex-LSMO, dextran-coated lanthanum strontium manganese oxide; RF, radiofrequency; SOD, superoxide dismutase; HSP, heat shock protein.

untreated control. However, catalase activity of the liver was not significantly altered in treated animals.

Effect of RF-induced Dex-LSMO nanoparticles-mediated hyperthermia treatment on induction of HSPs

To investigate whether Dex-LSMO nanoparticles-mediated hyperthermia can also lead to induction of HSPs, levels of HSP70 and HSP90 were evaluated. It could be seen that levels of both HSPs (Figure 8E and F) increased in treated tumors by approximately twofold as compared to the control, whereas levels of both HSPs in the liver of treated animals were not noticeably altered.

Discussion

The high zeta potential of Dex-LSMO nanoparticles indicated good colloidal stability and was in agreement with the results reported earlier.[14,15] Ferromagnetic nature and a low Curie

temperature indicated that Dex-LSMO nanoparticles were suitable for hyperthermia application.[14,15]

Tissue distribution data clearly showed that >50% of intra-tumorally injected Dex-LSMO nanoparticles get distributed and/or eliminated from tumor within 72 hours. Therefore, reinjection of Dex-LSMO nanoparticles after an interval of ~72 hours was necessary for hyperthermia regimen to achieve appropriate heating. Further, negligible accumulation of Dex-LSMO nanoparticles in healthy tissues indicated minimal risk of unwanted heating during hyperthermia treatment and confirmed the safety of the preparation. These data are in agreement with a study that reported the distribution of iron oxide nanoparticles in a mouse model where most of the nanoparticles were found to be retained in the tumor and negligible concentrations were detected in the liver and spleen.[21]

To date, iron oxide nanoparticles (magnetite) have been the most commonly used agent for RF-induced hyperthermia. Recently, LSMO nanoparticles have emerged as an alternative to iron oxide-based agents for hyperthermia. However, reports on tumor regression after LSMO nanoparticles-mediated hyperthermia are not available in the literature. Therefore, we compared our results with iron oxide nanoparticles-mediated hyperthermia. Balivada et al[1] reported that iron oxide nanoparticles (Fe_3O_4) injected at the site of tumor resulted in extensive cell death and tumor regression after exposure to repeated cycles of alternating magnetic field (5 kA/m, 366 kHz) for 10 minutes. Jordan et al[22] reported 4.5-fold prolongation of survival in glioblastoma-bearing rats after hyperthermia treatment using aminosilane-coated iron oxide nanoparticles. In another study, three cycles of hyperthermia using targeted iron oxide nanoparticles increased the survival by 31% in mice with pancreatic cancer.[23] Our results suggest that the efficacy of Dex-LSMO nanoparticles-mediated hyperthermia is comparable to that reported for iron oxide nanoparticles.

It is important to mention that tumor regression efficacy depends on initial tumor size as well as the number of hyperthermia cycles. For example, Ito et al[24] reported complete regression of small tumors (~7 mm) after a single cycle of hyperthermia at 45°C for 30 minutes, whereas complete regression of large tumors (~15 mm) needed multiple injections of Fe_3O_4 and up to six cycles of hyperthermia. It can, therefore, be proposed that increasing the cycles of Dex-LSMO nanoparticles-mediated hyperthermia may result in complete tumor regression.

Histological examination revealed necrotic areas in the tumor tissues of mice subjected to Dex-LSMO nanoparticles-mediated hyperthermia. Several studies have demonstrated tumor necrosis following hyperthermia.[25,26] For example, Nikfarjam et al[26] reported cell death and vascular injury after laser-induced hyperthermia treatment to the liver and colorectal metastases.

It is worth mentioning that Ki-67 is a nuclear protein expressed in all proliferating cells. It is a prognostic indicator of cancer[27] and can enable assessment of therapeutic efficacy. Therefore, several researchers have correlated antitumor efficacy with reduction in Ki-67 expression.[28,29] The observed reduction of Ki-67 expression in our study also establishes antitumor efficacy of Dex-LSMO nanoparticles-mediated hyperthermia.

Increased TUNEL signal in tumor of treated mice as compared to controls suggested apoptotic cell death. In the case of the liver tissue, the TUNEL signal across control groups and treated group was unaltered, indicating localized effect of Dex-LSMO nanoparticles-mediated hyperthermia. It is worth mentioning that TUNEL assay is not the sole indicator of apoptosis as the method can detect any type of DNA strand breakage.[26] DNA fragmentation by endonucleases is reported as a hallmark of the late events in apoptosis.[30] Thus, it was necessary to corroborate our findings with DNA laddering and caspase assays. In our study, the observed DNA laddering and activation of caspase-3 (a hallmark of final stage in apoptosis pathway) verified apoptotic mode of cell death induced by Dex-LSMO nanoparticles-mediated hyperthermia in melanoma-bearing mice. Also, lack of caspase activity in the liver suggested advantage of Dex-LSMO nanoparticles-mediated hyperthermia in the localized induction of apoptosis.

Researchers have reported apoptotic cell death after magnetic hyperthermia treatment of the lung carcinoma in nude mice[31] and B16F10 melanoma in C57BL/6J mice.[1] However, the exact mechanism of hyperthermia-induced apoptosis is not clearly defined yet. Several researchers have reported that hyperthermia in the range of 41°C–47°C usually induces signs of apoptosis, whereas higher temperatures >50°C are associated with tissue ablation by necrosis.[32,33] In agreement, our results showed that Dex-LSMO nanoparticles-mediated hyperthermia at ~45°C induced apoptosis in the tumor.

As reported in the literature, apoptosis is a clean pathway of cell death without involving inflammatory responses.[34] In agreement, the unaltered level of cytokines observed in our study confirmed apoptotic mode of cell death by Dex-LSMO nanoparticles-mediated hyperthermia.

Further, tumor SOD activity was unaltered after Dex-LSMO nanoparticles-mediated hyperthermia at ~45°C.

In agreement with our results, Arnaud et al[35] reported that a 15-minute heat stress at 42°C did not modify SOD activities of the myocardium in Wistar rats. Yoshioka et al[36] reported unaltered activity of SOD after hyperthermia that could be attributed to degradation of SOD by heat. Induction of catalase in treated tumor observed in our study indicates attenuation of oxidative stress, and indirectly suggests elevation of reactive oxygen species in the tumor after hyperthermia.

It is well known that cells respond to hyperthermia treatment by induction of HSPs, mainly HSP70 and HSP90.[37] Dex-LSMO nanoparticles-mediated hyperthermia resulted in HSP induction in tumors as compared to controls. In agreement with our results, Ito et al[38] reported that intra-tumorally injected iron oxide nanoparticles when exposed to alternating magnetic field for 30 minutes could induce cytoplasmic HSP70 immediately after treatment. It is important to mention that elevated levels of HSPs can render cells vigorous toward subsequent exposures to hyperthermia. This phenomenon is known as thermotolerance and might be misconstrued as a disadvantage for tumor treatment. Fortunately, thermotolerance is a temporary phenomenon and depends on the temperature applied and duration of hyperthermia.[39,40] If low temperature is applied for a short period (ranging from 10 to 30 minutes), cells try to survive by induction of HSPs (ie, thermotolerance), whereas beyond a certain temperature usually >43°C, despite a high level of induced HSPs, cells cannot sustain the heat stress and undergo apoptosis or necrosis. Released HSPs from the dead cells can trigger an antitumor immune response.[40]

The other advantage of hyperthermia-induced HSPs in treatment of cancer is that the induced HSPs can be specifically expressed on the surface of tumor cells but not on normal cells. These surface-expressed HSPs act as signals for the immune system and sensitize tumor cells for immune attack, resulting in "antitumor activity".[40] Jimbow et al[41] reported that melanoma-bearing mice treated with magnetite nanoparticles-mediated hyperthermia were able to reject rechallenge with melanoma. The authors attributed this observation to the development of antitumor activity by induction of HSP70 and HSP90. Thus, it can be proposed that similar phenomenon may occur after Dex-LSMO nanoparticles-mediated hyperthermia that may permit protection against relapse.

Conclusion

Dex-LSMO nanoparticles show promise as a novel heating agent for RF-induced hyperthermia. Further, restricted localization of Dex-LSMO nanoparticles in the tumor enables localized hyperthermia with minimal side effects to surrounding healthy tissues. To the best of our knowledge, this is the first study of its kind that demonstrates the utility of Dex-LSMO nanoparticles-mediated hyperthermia for cancer treatment in an animal model.

Acknowledgments

The authors thank G Mudliar and UA Risbud (Omega Scan Centre, Ratna Hospital, Pune, India) for MRI.

Disclosure

The authors disclose that there is no financial involvement with an organization or entity with a financial interest in or financial conflict with the subject matter or materials discussed in the paper.

References

1. Balivada S, Rachakatla RS, Wang H, et al. A/C magnetic hyperthermia of melanoma mediated by iron(0)/iron oxide core/shell magnetic nanoparticles: a mouse study. *BMC Cancer*. 2010;10(119):1–9.
2. Jia D, Rao W, Wang C, et al. Inhibition of B16 murine melanoma metastasis and enhancement of immunity by fever-range whole body hyperthermia. *Int J Hyperthermia*. 2011;27(3):275–285.
3. Jeon MJ, Ahn CH, Kim H, et al. The intratumoral administration of ferucarbotran conjugated with doxorubicin improved therapeutic effect by magnetic hyperthermia combined with pharmacotherapy in a hepatocellular carcinoma model. *J Exp Clin Cancer Res*. 2014;33(1):1–11.
4. Akbarzadeh A, Samiei M, Davaran S. Magnetic nanoparticles: preparation, physical properties, and applications in biomedicine. *Nanoscale Res Lett*. 2012;7(1):1–13.
5. Hegyi G, Szigeti GP, Szasz A. Hyperthermia versus oncothermia: cellular effects in complementary cancer therapy. *Evid Based Complement Alternat Med*. 2013;2013:672873.
6. Pollert E, Kaman O, Veverka P, et al. Core-shell $La_{1-x}Sr_xMnO_3$ nanoparticles as colloidal mediators for magnetic fluid hyperthermia. *Philos Trans R Soc A*. 2010;368(1927):4389–4405.
7. Chatterjee DK, Diagaradjane P, Krishnan S. Nanoparticle-mediated hyperthermia in cancer therapy. *Ther Deliv*. 2011;2(8):1001–1014.
8. Silva AC, Oliveira TR, Mamani JB, et al. Application of hyperthermia induced by superparamagnetic iron oxide nanoparticles in glioma treatment. *Int J Nanomedicine*. 2011;6(3):591–603.
9. Hilger I, Kaiser WA. Iron oxide-based nanostructures for MRI and magnetic hyperthermia. *Nanomedicine*. 2012;7(9):1443–1459.
10. Goya GF, Asin L, Ibarra RM. Cell death induced by AC magnetic fields and magnetic nanoparticles: current state and perspectives. *Int J Hyperthermia*. 2013;29(8):810–818.
11. Laurent S, Dutz S, Hafeli UO, Mahmoudi M. Magnetic fluid hyperthermia: focus on superparamagnetic iron oxide nanoparticles. *Adv Colloid Interface Sci*. 2011;166(1):8–23.
12. Martirosyan KS. Thermosensitive Magnetic Nanoparticles for Self-Controlled Hyperthermia Cancer Treatment. *J Nanomed Nanotechol*. 2012;3:112.
13. Kale SN, Aurora S, Bhayani KR, et al. Cerium doping and stoichiometry control for biomedical use of $La_{0.7}Sr_{0.3}MnO_3$ nanoparticles: microwave absorption and cytotoxicity study. *Nanomed Nanotechnol Biol Med*. 2006;2(4):217–221.
14. Bhayani KR, Kale SN, Aurora S, et al. Protein and polymer immobilized $La_{0.7}Sr_{0.3}MnO_3$ nanoparticles for possible biomedical applications. *Nanotechnology*. 2007;18(34):345101.
15. Haghniaz R, Bhayani KR, Umrani RD, Paknikar KM. Dextran stabilized lanthanum strontium manganese oxide nanoparticles for magnetic resonance imaging. *RSC Adv*. 2013;3(40):18489–18497.

16. Bhayani KR, Rajwade JM, Paknikar KM. Radio frequency induced hyperthermia mediated by dextran stabilized LSMO nanoparticles: *in vitro* evaluation of heat shock protein response. *Nanotechnology*. 2013; 24(1):015102.
17. Haghniaz R, Umrani RD, Paknikar KM. Temperature-dependent and time-dependent effects of hyperthermia mediated by dextran-coated $La_{0.7}Sr_{0.3}MnO_3$: *in vitro* studies. *Int J Nanomedicine*. 2015;10:1–15.
18. Villanueva A, de la Presa P, Alonso JM, et al. Hyperthermia HeLa cells treatment with silica coated manganese oxide nanoparticles. *J Phys Chem C*. 2010;114:1976–1981
19. Bubnovskaya L, Belous A, Solopan A, et al. Nanohyperthermia of malignant tumors. II. *In vivo* tumor heating with manganese perovskite nanoparticles. *Exp Oncol*. 2012;34(4):336–339.
20. Thorat ND, Otari SV, Patil RM, et al. Synthesis, characterization and biocompatibility of chitosan functionalized superparamagnetic nanoparticles for heat activated curing of cancer cells. *Dalton Trans*. 2014; 43(46):17343–17351.
21. Kettering M, Richter H, Wiekhorst F, et al. Minimal-invasive magnetic heating of tumors does not alter intra-tumoral nanoparticle accumulation, allowing for repeated therapy sessions: an *in vivo* study in mice. *Nanotechnology*. 2011;22(50):505102.
22. Jordan A, Scholz R, Maier-Hauff K, et al. The effect of thermotherapy using magnetic nanoparticles on rat malignant glioma. *J Neurooncol*. 2006;78(1):7–14.
23. Basel MT, Balivada S, Wang H, et al. Cell-delivered magnetic nanoparticles caused hyperthermia-mediated increased survival in a murine pancreatic cancer model. *Int J Nanomedicine*. 2012;7:297–306.
24. Ito A, Tanaka K, Honda H, Abe S, Yamaguchi H, Kobayashi T. Complete regression of mouse mammary carcinoma with a size greater than 15 mm by frequent repeated hyperthermia using magnetite nanoparticles. *J Biosci Bioeng*. 2003;96(4):364–369.
25. Wiersinga WJ, Jansen MC, Straatsburg IH, et al. Lesion progression with time and the effect of vascular occlusion following radiofrequency ablation of the liver. *Br J Surg*. 2003;90(3):306–312.
26. Nikfarjam M, Muralidharan V, Malcontenti-Wilson C, Christophi C. The apoptotic response of liver and colorectal liver metastases to focal hyperthermic injury. *Anticancer Res*. 2005;25(2B):1413–1420.
27. Fasching PA, Heusinger K, Haeberle L, et al. Ki67, chemotherapy response, and prognosis in breast cancer patients receiving neoadjuvant treatment. *BMC Cancer*. 2011;11(1):486.
28. Tan PH, Bay BH, Yip G, et al. Immunohistochemical detection of Ki67 in breast cancer correlates with transcriptional regulation of genes related to apoptosis and cell death. *Mod Pathol*. 2005;18(3): 374–381.
29. Ko SH, Ueno T, Yoshimoto Y, et al. Optimizing a novel regional chemotherapeutic agent against melanoma: hyperthermia-induced enhancement of temozolomide cytotoxicity. *Clin Cancer Res*. 2006;12(1): 289–297.
30. Collins RJ, Harmon BK, Gobe GC, Kerr JFR. Internucleosomal DNA cleavage should not be the sole criterion for identifying apoptosis. *Int J Radiat Biol*. 1992;61(4):451–453.
31. Hu R, Ma S, Li H, et al. Effect of magnetic fluid hyperthermia on lung cancer nodules in a murine model. *Oncol Lett*. 2011;2(6):1161–1164.
32. Cherukuri P, Glazer ES, Curley SA. Targeted hyperthermia using metal nanoparticles. *Adv Drug Deliv Rev*. 2010;62(3):339–345.
33. Milleron RS, Bratton SB. 'Heated' debates in apoptosis. *Cell Mol Life Sci*. 2007;64(18):2329–2333.
34. Cohen I, Rider P, Carmi Y, et al. Differential release of chromatin-bound IL-1α discriminates between necrotic and apoptotic cell death by the ability to induce sterile inflammation. *PNAS*. 2010;107(6):2574–2579.
35. Arnaud C, Joyeux M, Garrel C, Godin-Ribuot D, Demenge P, Ribuot C. Free-radical production triggered by hyperthermia contributes to heat stress-induced cardioprotection in isolated rat hearts. *Br J Pharmacol*. 2002;135(7):1776–1782.
36. Yoshioka A, Miyachi Y, Imamura S. Effects of local hyperthermia treatment on skin SOD activity in mice. *J Clin Biochem Nutr*. 1989;6(2): 109–115.
37. Bettaieb A, Wrzal PK, Averill-Bates DA. Hyperthermia: cancer treatment and beyond. In: Rangel L, editor. *Cancer Treatment – Conventional and Innovative Approaches*. Croatia: InTech publishers; 2013: 257–283.
38. Ito A, Shinkai M, Honda H, et al. Heat shock protein 70 expression induces antitumor immunity during intracellular hyperthermia using magnetite nanoparticles. *Cancer Immunol Immunother*. 2003;52(2): 80–88.
39. Griffin RJ, Ruud PMD, Jamshidi-Parsian A, Chang WS. Mild temperature hyperthermia and radiation therapy: role of tumor vascular thermotolerance and relevant physiological factors. *Int J Hyperthermia*. 2010;26(3):256–263.
40. Ito A, Honda H, Kobayashi T. Cancer immunotherapy based on intracellular hyperthermia using magnetite nanoparticles: a novel concept of "heat-controlled necrosis'' with heat shock protein expression. *Cancer Immunol Immunother*. 2006;55:320–328.
41. Jimbow K, Tamura Y, Yoneta A, et al. Conjugation of magnetite nanoparticles with melanogenesis substrate, NPrCAP provides melanoma targeted, *in situ* peptide vaccine immunotherapy through HSP production by chemo-thermotherapy. *J Biomater Nanobiotechnol*. 2012;3: 140–153.